







Article

# A New SLM-UFMC Model for Universal Filtered Multi-Carrier to Reduce Cubic Metric and Peak to Average Power Ratio in 5G Technology

Farooq Sijal Shawqi <sup>1</sup>, Lukman Audah <sup>1,\*</sup> , Salama A. Mostafa <sup>2,\*</sup> ,  
Saraswathy Shamini Gunasekaran <sup>3</sup>, Abdullah Baz <sup>4</sup> , Ahmed Talaat Hammoodi <sup>1</sup>,  
Hosam Alhakami <sup>5</sup> , Mustafa Hamid Hassan <sup>2</sup>, Mohammed Ahmed Jubair <sup>2</sup>  and  
Wajdi Alhakami <sup>6</sup> 

<sup>1</sup> Faculty of Electrical and Electronic Engineering, Universiti Tun Hussein Onn Malaysia, Johor 86400, Malaysia; He170090@siswa.uthm.edu.my (F.S.S.); Ge170131@siswa.uthm.edu.my (A.T.H.)

<sup>2</sup> Faculty of Computer Science and Information Technology, Universiti Tun Hussein Onn Malaysia, Johor 86400, Malaysia; Gi170006@siswa.uthm.edu.my (M.H.H.); Gi170009@siswa.uthm.edu.my (M.A.J.)

<sup>3</sup> College of Computing and Informatics, Universiti Tenaga Nasional, Selangor 43000, Malaysia; sshamini@uniten.edu.my

<sup>4</sup> Department of Computer Engineering, College of Computer and Information Systems, Umm Al-Qura University, 21955 Makkah, Saudi Arabia; aobaz01@uqu.edu.sa

<sup>5</sup> Department of Computer Science, College of Computer and Information Systems, Umm Al-Qura University, 21955 Makkah, Saudi Arabia; hhhakam@uqu.edu.sa

<sup>6</sup> Department of Information Technology, College of Computers and Information Technology, Taif University, 21944 Taif, Saudi Arabia; whakami@tu.edu.sa

\* Correspondence: hanif@uthm.edu.my (L.A.); salama@uthm.edu.my (S.A.M.);  
Tel.: +60-143844550 (L.A.); +60-1123231938 (S.A.M.)

Received: 1 April 2020; Accepted: 7 May 2020; Published: 1 June 2020



**Abstract:** The new generation of wireless communication systems has adopted different waveforms. The universal filtered multicarrier is one of the adopted candidates that has symmetry with various numerology designs. However, the high peak to average power ratio is one of the major limitations faced by universal filter multicarrier (UFMC) designers. Moreover, recent studies utilize cubic metric along with the peak to average power ratio (PAPR) to show the power back-off effect of the signal in which the PAPR metric identifies the maximum peak and the cubic metric (CM) identifies the Out of Band emission and In-Band distortion. Most of the current solutions, such as amplitude clipping, tone reservation, and active constellation extension, decrease the PAPR but cause degradation to the bit error rate. Selected mapping is one of the promising techniques that is recently used to solve the PAPR and CM problems without causing bit error rate (BER) degradation. In this paper, the selected mapping (SLM) is integrated with UFMC to reduce the PAPR and CM without affecting the BER of 5G networks. The SLM-UFMC solution model is simulated by MATLAB and the results show that the SLM-UFMC model presents better PAPR and CM performance without BER degradation. The PAPR has been decreased to 1.5 dB with respect to eight-phase rotation vectors and the CM decreased to 1.25 dB compared to the conventional UFMC.

**Keywords:** universal filter multicarrier (UFMC); selected mapping (SLM); peak to average power ratio (PAPR); cubic metric (CM); bit error rate (BER); cumulative distributive function (CDF)

## 1. Introduction

In the current applications of cellular devices, there is a great demand for incorporating 5G networks as a replacement for the 4G type. Generally, the Machine to Machine (M2M), Device to Device

(D2D), massive Machine Type Communications (mMTC) and mobile phone technologies improve instantly [1]. The 5G solution provides the means to satisfy advanced networking in terms of high bandwidth capacity, traffic rate, availability and connectivity [2]. The enhanced Mobile Broadband (eMBB) is an extension of the mobile broadband telecommunication standards. It provides multiple connectivity (e.g., hotspot or wide-area coverage) with high data rates of services and multimedia data. Ultra-Reliable Low Latency Communications (URLLC) are used for machine-type communications and provide better latency and reliability. Its applications include distribution automation in smart grids, industrial manufacturing and remotely driven vehicles. The mMTC provides massive connectivity with a low amount of traffic and possible delays. Its applications include Internet of Things (IoT) systems [1]. These three communication approaches manifest the dimensions of features in the 5G network, as shown in Figure 1.

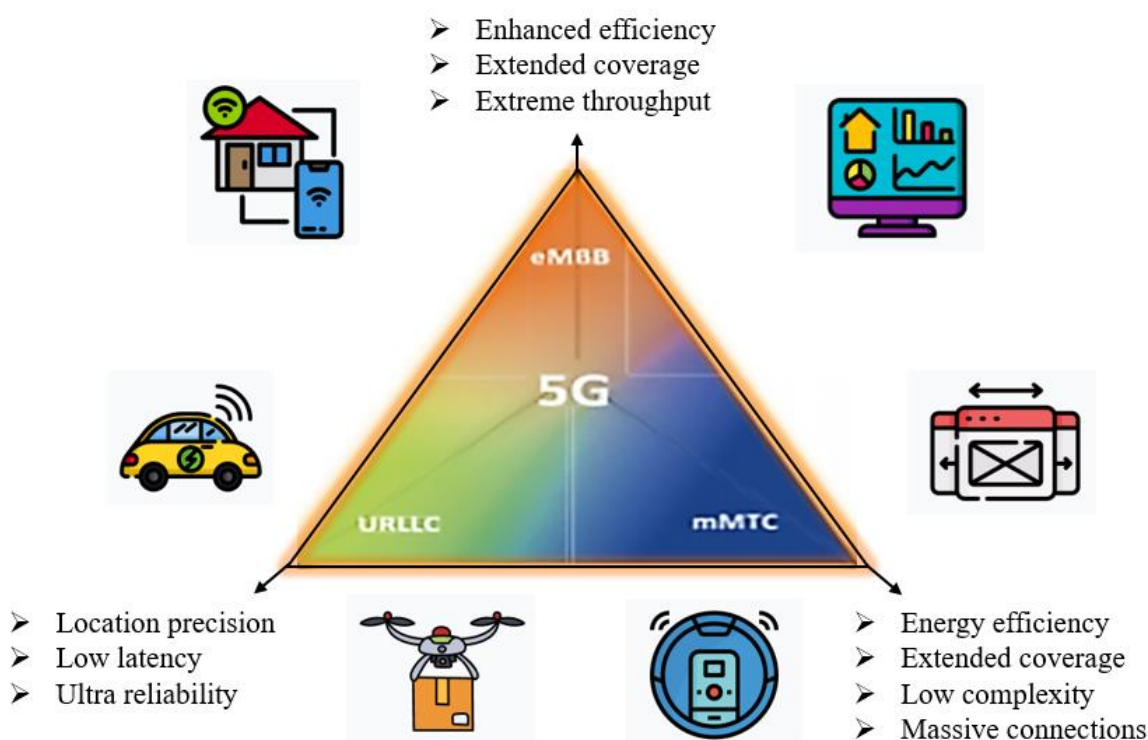


Figure 1. The main features of the 5G networks.

The communications standards of the waveform networks advancement entail different structures, modulation symbol formats and/or sizes [3]. Some examples are Frequency Division Multiplexing (FDM), Orthogonal Frequency Division Multiplexing (OFDM) and the advanced Cyclic Prefix-OFDM (CP-OFDM). The CP-OFDM has been commercially deployed in 4G as a Long-Term Evolution (LTE) technology [4]. However, in LTE, CP-OFDM failed to support the demands of different numerologies and communication scenarios. There are a few other multiplexing types, such as Generalized Frequency Division Multiplexing (GFDM) [5], non-orthogonal multiple access [6], Filter Bank Multicarrier (FBMC) [7–9], filtered OFDM (f-OFDM) [10], and Universal Filtered Multicarrier (UFMC), which is also called universal filtered OFDM (UF-OFDM) [11]. The UFMC is considered as the most suitable waveform for 5G technology [12].

The main defect of multicarrier modulation schemes is the high Peak to Average Power Ratio (PAPR) due to the coherence of subcarriers in the time-domain [13]. High PAPR drives the power amplifier to the non-linearity region [12,13], which leads to Out of Band (OOB) emission, In-Band (IB) distortions and long word length. The long word length is an essential problem in the digital to analogue converter, which dramatically reduces battery life. Various solutions are proposed to reduce the PAPR in the waveform. Amplitude clipping is the simplest non-linear time-domain located method.

The amplitude clipping reduces the OOB emission and IB distortion but increases the BER [14,15]. Companding is another time-domain-located method that reduces PAPR. It compresses the large peaks and enlarges the small peaks of the signal but increases the BER too [16–18].

On the other hand, frequency-domain methods such as Tone Reservation (TR) and Tone Injection (TI) support PAPR reduction [19–21]. However, TR and TI consume high power and processing time to find the optimum cancellation tones. A Multiple Signal Representation (MSR) is another frequency-domain method that solves the PAPR problem. The MSR is a probabilistic method that generates and transmits multiple copies of original data vectors, which reduce the PAPR but increases the BER [22].

Partial Transmit Sequences (PTS) [23] and Selected Mapping (SLM) [24] are two methods that belong to both time- and frequency-domains and assist in PAPR reduction. They use a statistical mechanism that avoids increasing the BER. However, the PTS needs more side information than the SLM, which decrease the capacity of the transmitted data and causes data rate reduction. Hence, the SLM is extensively integrated with different waveforms [16]. For example, Figure 2 shows the SLM and CP-OFDM integration in which multiple copies or branch of the original data are generated. Each copy is multiplied by the corresponding phase rotation vector,  $p^i$  ( $1, 2, \dots$ ). In Figure 2, the fast version Inverse Fast Fourier Transform (IFFT) is used to transform between frequency- and time-domains. The branch with minimum PAPR is adopted for transmission along with the needed side information. This side information is a strongly protected small number of binary bits that guarantee correct data recovery at the receiving end [25,26]. However, side information protection and transmitting are not within the scope of this work.

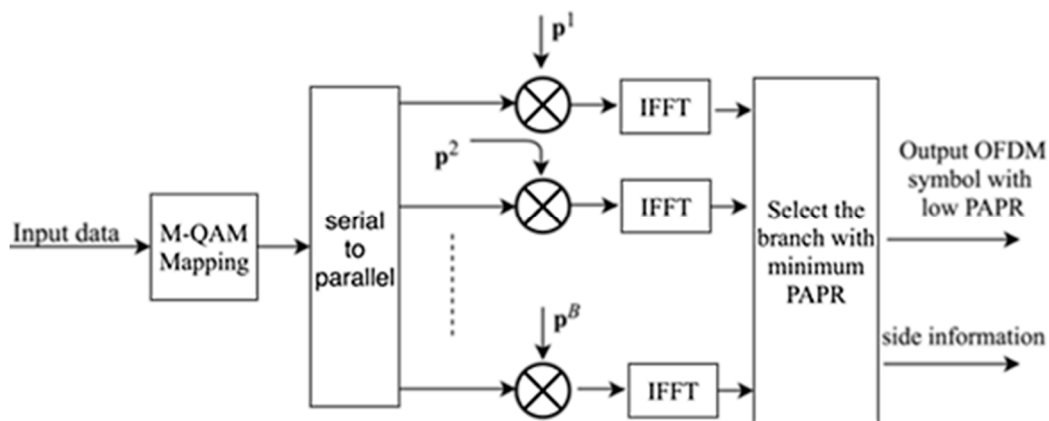


**Figure 2.** Cyclic Prefix Orthogonal Frequency Division Multiplexing (CP-OFDM-based Selected Mapping (SLM) scheme.

On the other hand, because of the computational complexity of the SLM, different modified versions of SLM are suggested [27–29]. The aim of modifying the SLM method is to reduce the computational complexity, while keeping the probabilistic nature, i.e., less BER degradation. Generally, the modification either degrades the BER performance or the PAPR performance, thus, there is a trade-off between the computational complexity, the PAPR and the BER degradation. For instance, Jeon et al. [27] built the SLM scheme in the time-domain of the OFDM waveform and add the rotating sets to the signals. The version of SLM show low complexity results and improve the BER, however the PAPR is increased significantly. According to the periodic properties of the IFFT transform, it is possible to generate conversion matrices in the time-domain, such that the time-domain OFDM signal is multiplied by these conversion matrices to reduce the computational complexity. The drawback point of this approach is limiting the transformed data rate (i.e., the BER), which leads to an increase in the transmission cycle and energy consumption [30]. Hu et al., [31] implemented the chaos phase rotation vectors (CPRV) in the conventional SLM method. The method reduces the PAPR but increases

the computational complexity [32]. Contrarily, the work of Wang and Akansu [33], reduces the computational complexity but increases the PAPR. Furthermore, the work of Wang et al. [34] shows that translating the SLM operations from the frequency-domain side to the time-domain side can be a key aspect to reducing the computational complexity. In Hu et al., [35] multiple candidates are generated in the time-domain using conversion matrices and IFFT properties. The computational complexity is reduced by around 50% at the expense of PAPR reduction gain degradation and BER performance degradation.

The candidate multiplexing systems have a different structure to the traditional CP-OFDM systems. Thus, distinct versions of SLM for this type are shown in the literature, such as over-lapp-SLM (OSLM) [20], dispersive SLM [36], and Trellis-SLM [37]. However, these versions are all suggested for the FBMC. Furthermore, tone-reservation-based SLM [38] and windowed SLM [39] are proposed for the FBMC and reduce the PAPR. To the best of our knowledge, SLM for the UFMC waveform has not been proposed and evaluated. This study indicates that SLM has better spectral efficiency and can be used to reduce the Inter-Carrier Interference (ICI), which is symmetrical with the improvement of the UFMC signals.

The UFMC system is one of the new candidate waveforms for 5G systems. UFMC is expected to achieve low latency, robustness against frequency offset, and reduce out-of-band (OoB) radiation, which leads to higher spectral efficiency. Although the UFMC system offers many advantages, as mentioned before, being a multicarrier transmission technology, it suffers from high PAPR [8]. Hence, in this paper, the SLM is proposed to be integrated with the UFMC signals. Consequently, the mathematical model of the SLM-UFMC method is presented and the PAPR, BER and computational complexity are evaluated. The Cubic Metric (CM) is used to estimate the method performance concerning the nonlinearity of the high-power amplifier. The CM is used by [40–44] to find the effect of the power amplifier on the signal.

The rest of this paper is organized as follows. The methods and materials are presented in Section 2. The mathematical models for the proposed method SLM-UFMC are presented in Section 3. The results and discussion are presented in Section 4. Finally, the research conclusion and future work are presented in Section 5.

## 2. Materials and Methods

### 2.1. Simulation Model and Parameters

The experimental tests of the simulation aim to improve the 5G performance by decreasing the PAPR and BER. The SLM-UFMC is proposed to find the optimum wave with the lowest PAPR and CM levels. Afterwards, three existing waveforms are tested via simulation program and the results are compared with the SLM-UFMC. Figure 3 represents the main steps that are used to implement the simulation of the SLM-UFMC and the other waveforms. The simulation model consists of five main modules. Firstly, the 5G environment Module A is employed to create simulation environments. This module integrates the main characteristics of 5G, such as data rate, packet size and a number of devices. Module B represents the implementation of the SLM-UFMC model and the existing UFMC [11] and SLM-CP-OFDM [20] models. In this module, several windows have been included to address the progress of the solutions. In Module C, different numbers of QAMs (e.g., four, eight, 16, 64, 256) are employed to generate testing scenarios with various states to comprehensively assess the performance of the proposed model compared with the tested waveforms. The scenarios are altered in each set of runs of a particular waveform. In Module D, the performance metrics of CCDF and BER are implemented to evaluate the SLM-UFMC, SLM-CP-OFDM, and conventional UFMC. Finally, Module E depicts the results and visualization graphs in a windows form.

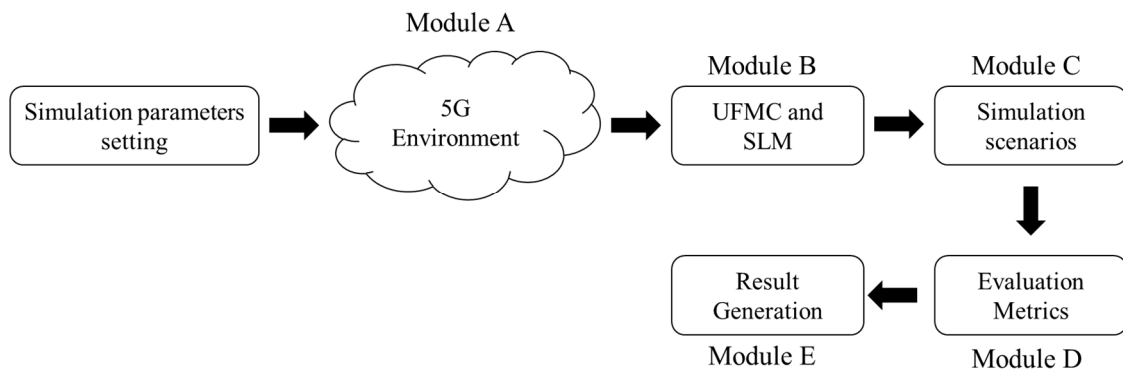


Figure 3. Simulation design.

## 2.2. The Evaluation Metric

Complementary Cumulative Distributive Function (CCDF) denotes the probability that the PAPR of a data block exceeds a given threshold ( $PAPR_0$ ) [45] and is expressed as follows

$$CCDF[PAPR(x_n)] = prob(PAPR(x_n) > PAPR_0) \quad (1)$$

The Bit Error Rate (BER) is the number of bit errors divided by the total number of transferred bits during a studied time interval [45]. It is often expressed as a percentage and it has no measurement unit.

$$BER = \frac{N_{Err}}{N_{bits}} \quad (2)$$

## 3. Mathematical Models

### 3.1. UPMC System Model

In 5G, UPMC is a novel multicarrier modulation of QAM type that represents an alternative to the OFDM and FBMC waveforms. Unlike self-subcarrier modulation in FBMC, a group of subcarrier modulation is performed in UPMC. The subcarrier grouping reduces the length of the filter compared with FBMC and also reduces the performance time. Starting from the traditional OFDM system, UPMC can be considered as a generalized version of the OFDM. Let the OFDM be formulated based on Equation (3)

$$x(k) = \frac{1}{\sqrt{N}} \sum_{n=0}^{N-1} X(n) e^{j2\pi \frac{nk}{N}} \quad (3)$$

where  $x$  is the OFDM signals that represent an IDFT of size  $N$ ;  $k$  stands for the time index;  $n$  represents the frequency-domain index;  $X$  set is generated based on quadrature multi-level amplitude modulation (M-QAM) mapping. The  $X$  set contains Identically Independent Distributed (IID) random variables. The summation in Equation (1) is either constructive or destructive. Thus, the coherence summation of data will result in a large peak compared with the average, which is called the peak to average power ratio. The CP-OFDM (i.e., cyclic-prefix free) that is adopted in LTE can be formed by adding the filter to the whole band, as in Equation (1). Executing the filter in Equation (4) gives the CP-OFDM

$$x = W \cdot X \quad (4)$$

where  $W$  is the IDFT matrix of size  $N \times N$ , where  $N$  is the number of subcarriers. Subsequently, we formed Equation (5)

$$x = F \cdot W \cdot X \quad (5)$$

where  $F$  stands for the Finite Impulse Response (FIR) filter toeplitz matrix, which achieves the convolution operation over the band of  $N$ . If the whole band subdivided to  $R$  sub-bands, then, the UFMC system can be expressed as Equation (6)

$$x = \sum_{r=1}^R F_r \cdot W_r \cdot X_r \tag{6}$$

In Equation (6), the M-QAM symbols entries of  $X_r$  are first converted to the time-domain according to the corresponding column of IDFT matrix  $W_r$  which corresponds to the specified sub-band  $r$  within the frequency band.  $F_r$  is the corresponding sub-band filter. Figure 4 depicts the complete UFMC system that is derived from Equation (6). In the receiver end, the process starts at the zero-padding to achieve the two times up-sampling. Then, conducting the 2N-DFT, the subcarriers (down-sampling) of a juncture are selected, until the M-QAM de-mapping is implemented to collect the received data, as shown in Figure 4. The next section illustrates the integration of the selected mapping method with the UFMC waveform.

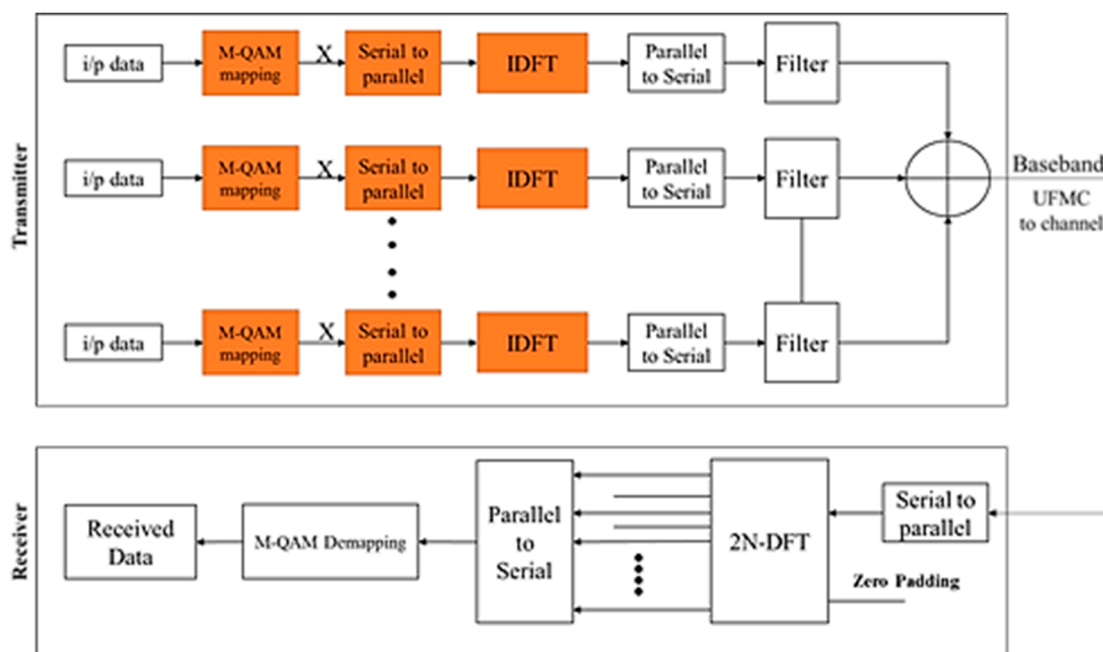


Figure 4. Universal Filtered Multicarrier (UFMC) baseband transceiver.

Based on Figure 4, the filtering operation has a block-wise form of Physical Resource Block (PRB) to facilitate the flexibility of the design. The filter length has an essential role in the design of the system in which the filter length,  $P \gg 1$  and  $X$  contain one M-QAM symbol. As long as the filter length in the frequency-domain is long, the time-domain tail is going to be shorter (i.e., in the order of cyclic prefix length of the traditional CP-OFDM), which enables the network to support Transmits Short Messages (TSM). Additionally, the elimination of the sidelobes is conducted at the ends of the sub-bands not between the subcarriers, as in the case of the FBMC signal structure. The ramping up/down in the time-domain gives more shields to prevent inter-symbol interference (ISI). Unlike the FBMC, the UFMC keeps the complex orthogonality, thus the Multiple-Input-Multiple-Output (MIMO) mechanism of multiple users is efficiently implemented in the UFMC. On the other hand, the UFMC is more efficient than CP-OFDM in terms of spectrum construct, due to the UFMC being CP-free. At the receiving end, the process starts at the zero paddings to achieve a two times up-sampling. Then, when conducting the 2N-DFT after that point and while selecting every other subcarrier, which is down-sampling, UFMC

can achieve M-QAM de-mapping to collect the received data, as shown in Figure 4. At this stage, PAPR can be formulated as follows

$$PAPR = 10 \log_{10} \left[ \frac{\max |x(k)|^2}{E[|x(k)|^2]} \right] \quad (7)$$

where  $E[|x(k)|^2]$  is the expectation operation, which gives the average power of the signal  $x(k)$ . The HPA reaches the saturation region if high peaks are fed to it, thus it causes degradation in the system. Therefore, such high peaks have to be reduced. Recently, it is found that the PAPR metric alone is not enough to predict the HPA power de-rating, thus the CM is proposed as a sporting metric in the 3GPP [41].

$$CM = \frac{20 \log_{10} \{rms[x_{norm}^3(k)]\} - 20 \log_{10} \{rms[x_{ref}^3(k)]\}}{K} \text{ dB} \quad (8)$$

where  $20 \log_{10} \{rms[x_{norm}^3(k)]\}$  represents the raw Cubic Metric (rCM) of the signal  $x(k)$  and  $20 \log_{10} \{rms[x_{ref}^3(k)]\}$  is a constant reference that represents the rCM of Wide-Code Division Multiple Access (W-CDMA) voice signals [41]. The reference signal is found to be 1.25 dB [40,41]. The denominator stands for the empirical slope factor, which is determined empirically for a wide range of signals proposed for LTE applications to be 1.56. Furthermore,  $rms(x)$  can be calculated from.

$$rms = \sqrt{\frac{x^*x}{N}} \quad (9)$$

and

$$x_{norm}(k) = \frac{|x(k)|}{rms(x(k))} \quad (10)$$

where  $x$  denotes the vector form of the signal of [2,6]. That is, HPA power back-off affects the system performance, which is called power de-rating (the HPA operation is described in [40]). The HPA nonlinearity produces Adjacent Channel Leakage Ratio (ACLR), which is the ratio of mean power assigned to a certain channel with the mean power assigned to the adjacent channel. In the specifications of the LTE systems, it is found that the ACLR is 30 dB-sufficient for proper operation [46].

$$v_o(t) = G_1 v_i(t) + G_3 v_i^3(t) \quad (11)$$

where  $G_1$  and  $G_2$  are the linear and cubic gain design factors of the power amplifier. The power de-rating of a power amplifier is the amount of back-off power required to meet the ACLR specification of the transmitting system. Thus, the second term of the last expression shows the nonlinearity source in the power amplifier, which is the main source of the ACLR. Assuming the input of the HPA in the last expression has two consecutive frequencies, then

$$x_{1,2}(k) = A_1 e^{j\theta_1} + A_2 e^{j\theta_2} \quad (12)$$

where  $\theta_1 = 2\pi k \frac{a}{N}$  and  $\theta_2 = 2\pi k \frac{b}{N}$ , in which  $a$  &  $b$  are two adjacent frequency indices, and  $A_1$  &  $A_2$  are the two corresponding constellation points data. Then, the last expression of the two adjacent frequencies becomes

$$x_{1,2}(k) = G_1 [A_1 e^{j\theta_1} + A_2 e^{j\theta_2}] + G_3 [A_1 e^{j\theta_1} + A_2 e^{j\theta_2}]^3 \quad (13)$$

Expanding the cubic term yields

$$x_{1,2}(k) = G_1 [A_1 e^{j\theta_1} + A_2 e^{j\theta_2}] + G_3 [A_1^3 e^{j3\theta_1} + A_2^3 e^{j3\theta_2} + 3A_1^2 A_2 e^{j(2\theta_1+\theta_2)} + 3A_1 A_2^2 e^{j(\theta_1+2\theta_2)}] \quad (14)$$

where the first term stands for the fundamental signal frequencies which is a linear region that can be inferred from the PAPR value and the second term involves the nonlinear frequencies. The terms of the last expression ignore other the effect of other terms  $(3A_1^2A_2e^{j(2\theta_1+\theta_2)} + 3A_1A_2^2e^{j(\theta_1+2\theta_2)})$ , which make an essential motivation to introduce the ACLR [40,41,46]. Thus, the intermodulation is happened due to the cubic terms, which produce  $2\theta_1 + \theta_2$  and  $\theta_1 + 2\theta_2$  frequencies. Hence

$$x(k) = G_1 \sum_{n=0}^{N-1} X_n e^{j2\pi k \frac{n}{N}} + G_3 \sum_{n=0}^{N-1} (X_n^3 e^{j2\pi k \frac{3n}{N}} + X_{n+1}^3 e^{j2\pi k \frac{3n+3}{N}}) + 3G_3 \sum_{n=0}^{N-1} \sum_{c=1}^{N-n-1} (X_n^2 X_{n+c} e^{j2\pi k \frac{n+c}{N}} + X_n X_{n+c}^2 e^{j2\pi k \frac{n+2c}{N}}) \tag{15}$$

From (14) and (15), it can be verified that the real cause of ACLR is the third intermodulation term. Thus, the cubic metric will be more accurate than the PAPR metric to determine the power amplifier power back-off. It can be seen that the PAPR predicts the envelope fluctuation of the linear region only, while CM predicts the other orders of the HPA operation regions. Hence, in this work, both two metrics, PAPR and CM, will be conducted to check the power back-off effect on the system using the SLM method.

### 3.2. UPMC Based SLM System

The SLM algorithm is one of the efficient frequency-domain approaches to reduce the PAPR in OFDM waveform. Basically, the algorithm applies a mechanism to make  $B$  copies of the M-QAM modulated data vector, multiply elementwise, phase rotation vectors [32]. Based on the colored blocks in Figure 4, after phase rotation vector implementation, the  $X$  in (6) takes the form

$$X_r^b = p^b \times X_r \tag{16}$$

where

$$X_r^b = \begin{bmatrix} X_{r,0}^b \\ X_{r,1}^b \\ \vdots \\ X_{r,N-1}^b \end{bmatrix}, \quad p^b = \begin{bmatrix} p_0^b & 0 & \cdots & 0 \\ 0 & p_1^b & \cdots & 0 \\ \vdots & \vdots & \ddots & 0 \\ 0 & 0 & \cdots & p_{N-1}^b \end{bmatrix}, \quad X_r = \begin{bmatrix} X_{r,0} \\ X_{r,1} \\ \vdots \\ X_{r,N-1} \end{bmatrix} \tag{17}$$

and  $b$  stands for the phase rotation vector  $p$  index. Then, the UPMC-based SLM can be expressed as

$$x^b = \sum_{r=1}^R F_r \cdot W_r \cdot [p^b \times X_r] \tag{18}$$

or

$$x^b = \sum_{r=1}^R F_r \cdot W_r \cdot X_r^b \tag{19}$$

In other words, UPMC-based SLM now produces  $B$  candidates, the candidate who experiences lower PAPR will be adopted for transmission. The QAM-Mapper produces data then copies the data multiple times to phase-rotate it. In the above scenario, shown in Equation (17), the computational complexity can be calculated as that of the conventional CP-OFDM. For instance, the number of complex multiplication operations of the CP-OFDM matches that of the UPMC, as well as the number of complex addition operations [47]. Hence, the number of complex multiplication operations  $\mu$  can be presented as Equation (20)

$$\mu = \frac{N}{2} \log_2(N) \tag{20}$$



where  $N$  refers to the number of samples, then according to [47], the number of complex addition operations can be formed as in Equation (21)

$$\alpha = N \log_2(N) \quad (21)$$

After implementing the PAPR/CM reduction approach, which is represented by the SLM scheme, the number of complex multiplication operations will be increased according to the number of candidates,  $B$ ,

$$\mu_{SLM} = B \frac{N}{2} \log_2(N) \quad (22)$$

The  $\alpha_{SLM}$ , calculated by multiplying the number of complex addition operations (as shown in Equation (21)) by  $B$ , in which the  $B$  refers to the total number of SLM candidates:

$$\alpha_{SLM} = BN \log_2(N) \quad (23)$$

On the other hand, the SLM scheme is the probabilistic method, hence the BER is not affected. Although the computational complexity has been increased, the achieved outcome is of great interest. Moreover, SLM needs to transmit some side information to the receiver, such that the data can be recovered. The amount of side information is a few bits, which can be calculated as Equation (24):

$$\delta = \log_2(B) \quad (24)$$

In other words, decreasing the number of candidates decreases the reserved bits as side information and reduces the computational complexity at the same time. Hence, it is worth controlling the number of candidates in order to obtain improved results. Thus, there is a trade-off between the reduction performance and the computational complexity. These facts are validated by conducting the mathematical simulations, and their outcomes are presented in Section 3.

#### 4. Results and Discussion

This work presents four scenarios that are carried out according to constellation order  $M$ . Table 1 lists briefly the utilized parameters in the consequent simulations. As shown in Table 1, there are 20 PRBs, each PRB contains 14-subcarriers, and each subcarrier is modulated with QPSK, 16-QAM, 64-QAM, and 256-QAM i.e., there are 2-, 4-, 6-, and 8-binary bits of a message in the four scenarios, respectively. These parameters are chosen according to the LTE standards [47]. Moreover, there is 4-, 6-, and 8-PRV in each scenario. Figure 5a,b shows the simulation results according to the first line entries of Table 1, in which 4-PRV and QPSK mapping are used.

**Table 1.** Simulation parameters for SLM-CP-Orthogonal Frequency Division Multiplexing (OFDM), SLM-UFMC, and conventional UFMC.

N Size of IFFT	No. of Subcarriers	No. of PRB	M Constellation Order	No. of PRV
512	14	20	4	4, 6, and 8
512	14	20	16	4, 6, and 8
512	14	20	64	4, 6, and 8
512	14	20	256	4, 6, and 8

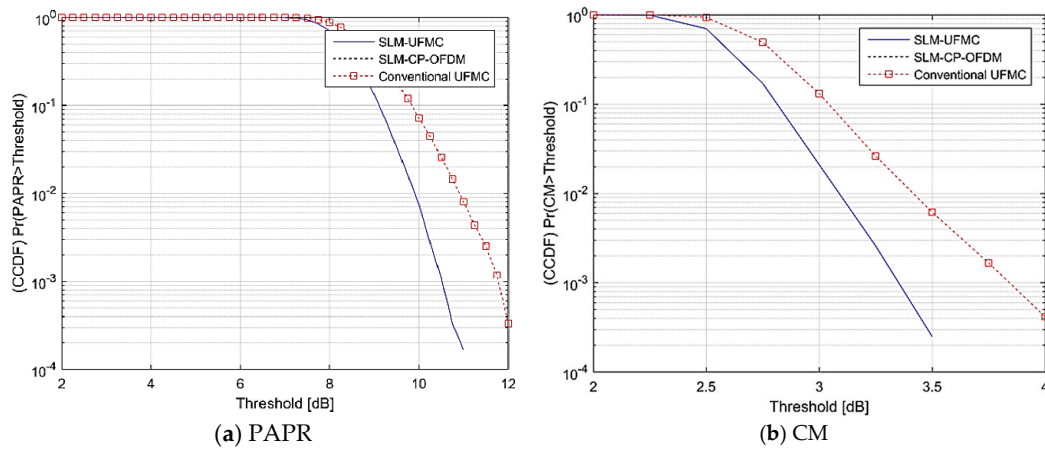


**Figure 5.** The 4-Quadrature Amplitude Modification (QAM) and 4-Phase Rotation Vector (PRV) results of scenario 1.

From Figure 5a, it is obvious that the QPSK or 4-QAM mapping does not take shape in the results. This behavior is due to the QPSK/4-QAM mapping has already low PAPR or CM, thus, after implementing the SLM method, the PAPR of the CP-OFDM vanished. While the conventional UFMC has a higher PAPR than the conventional CP-OFDM, it is 12 dB. Interestingly, after selected mapping, the SLM-UFMC experiences lower PAPR of 11 dB, in which there is a 1 dB reduction in the PAPR when using 4-PRV. On the other hand, the cubic metric, which is shown in Figure 5b, shows the same outcomes as that of the PAPR in Figure 5b with respect to SLM-CP-OFDM QPSK/4-QAM mapped signals. However, the conventional UFMC produces a higher CM value, 4 dB, while the SL-UFMC acts better with 4-PRV, at 3.5 dB, thus a reduction in 0.5 dB in the CM is achieved. For this scenario, the SLM-UFMC shows better performance and consumes less power than the SLM-CP-OFDM and conventional UFMC.

In Figure 6a,b, the PAPR and CM of 6-PRV Rotation Vectors (PRV) are compared using the settings of the same signal of the previous configuration. The SLM-UFMC achieves a 1 dB and 0.75 dB reduction in the PAPR and CM, respectively. For the 8-PRV, the SLM-UFMC reduces the PAPR from 12 to 10.75 dB and enhances the CM by 0.75 dB. As a result, the CM with 8-PRV does not improve too much compared with the 6-PRV rotation vectors, as shown in Figure 7a,b. Thus, for this scenario, it is recommended to use a maximum of 6-PRV rotation vectors, as shown in Table 2. Although the PAPR is reduced by 1.25 dB, the effect of the third intermodulation, which causes the ACLR, can be accurately captured by the CM approach.

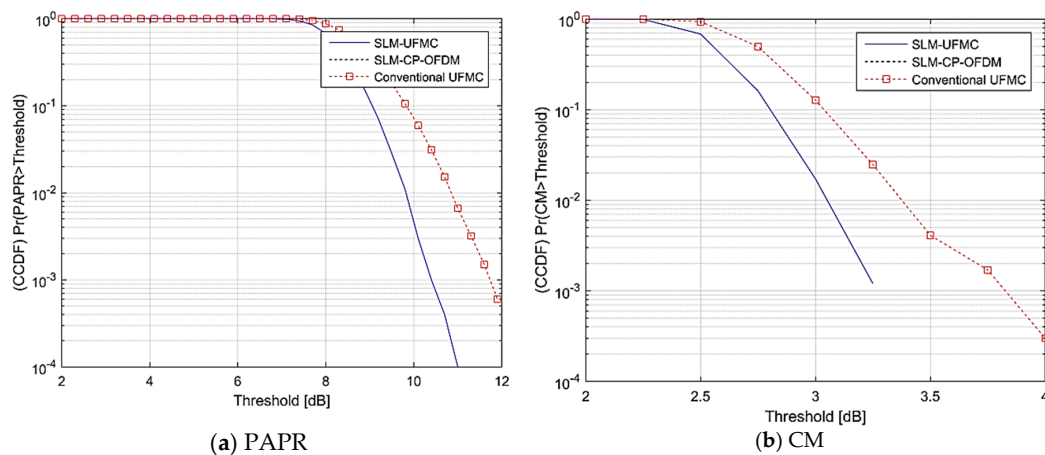


**Figure 6.** The 4-QAM and 6-PRV results of scenario 1.

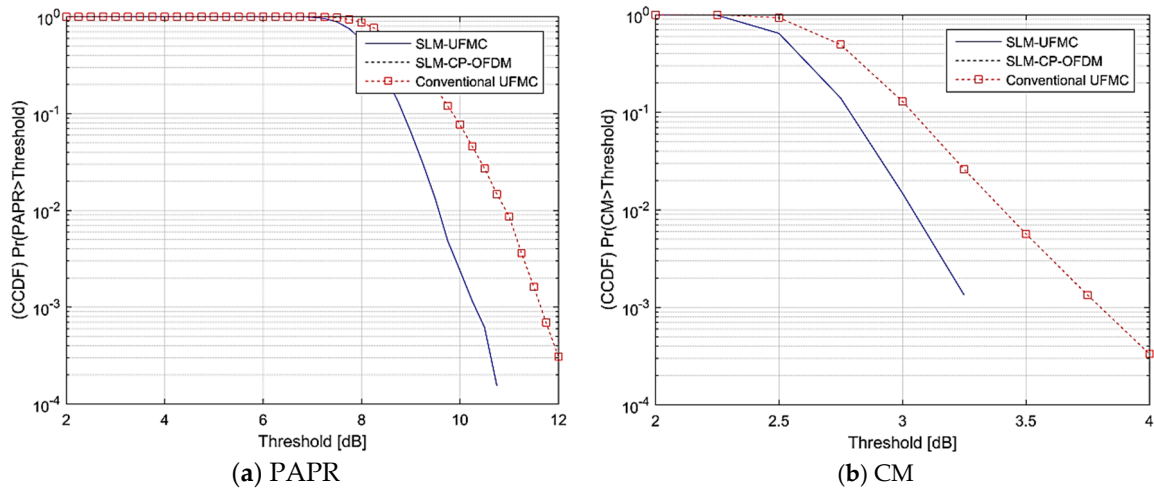


Figure 7. The 4-QAM and 8-PRV results of scenario 1.

Table 2. Simulation results for the first scenario (QPSK/4-QAM), SLM-UFMC, and conventional UFMC.

No. of PRV	PAPR Before Reduction in dB	CM Before Reduction in dB	PAPR After Reduction in dB	CM After Reduction in dB	PAPR Reduction in dB	CM Reduction in dB
4	12	4	11	3.5	1	0.5
6	12	4	11	3.25	1	0.75
8	12	4	10.75	3.25	1.25	0.75

In the second scenario of Table 1, the modulation order is increased to four binary bits in each subcarrier, and hence the 16-QAM mapping is conducted in its simulations. With 16-QAM and 4-PRV, the conventional UFMC reduces the PAPR and CM from 12 and 4 dB to 10.75 and 3.5 dB, respectively. Subsequently, the SLM-UFMC reduces the PAPR and CM to 1.25 dB and 0.5 dB as shown in Figure 8a,b. The SLM-CP-OFDM shows better PAPR performance than SLM-UFMC, but at the cost of spectrum deficiency.

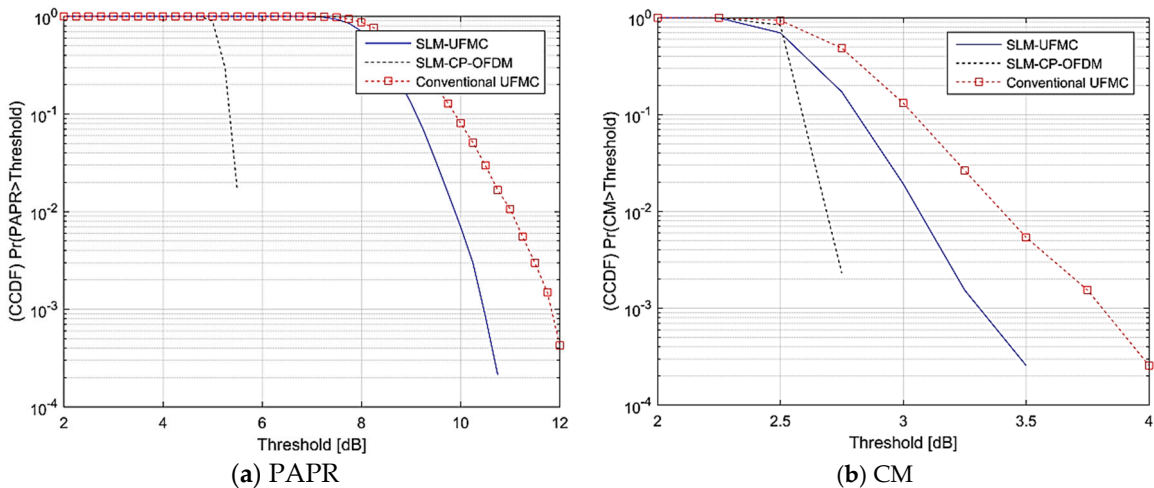


Figure 8. The 16-QAM and 4-PRV results of scenario 2.

In the same scenario of 16-QAM, the number of PRV increased to six (6-PRV). Figure 9a shows that the PAPR of the conventional UFMC is 12.25 dB. The PAPR is reduced to 11 dB, with a reduction of 1.25 dB. The CM in Figure 9b of the conventional UFMC is 4.25 dB, while in the SLM-UFMC, it drops to 3.5 dB, with a reduction of 0.75 dB. It can be seen that using 4- or 6-PRV does not make a significant

change in the PAPR and CM, as shown in Table 3. The SLM-CP-OFDM in both cases has a greater reduction in the PAPR and CM, but it is impossible to use CP-OFDM for different numerologies, which is why we are seeking other waveforms.

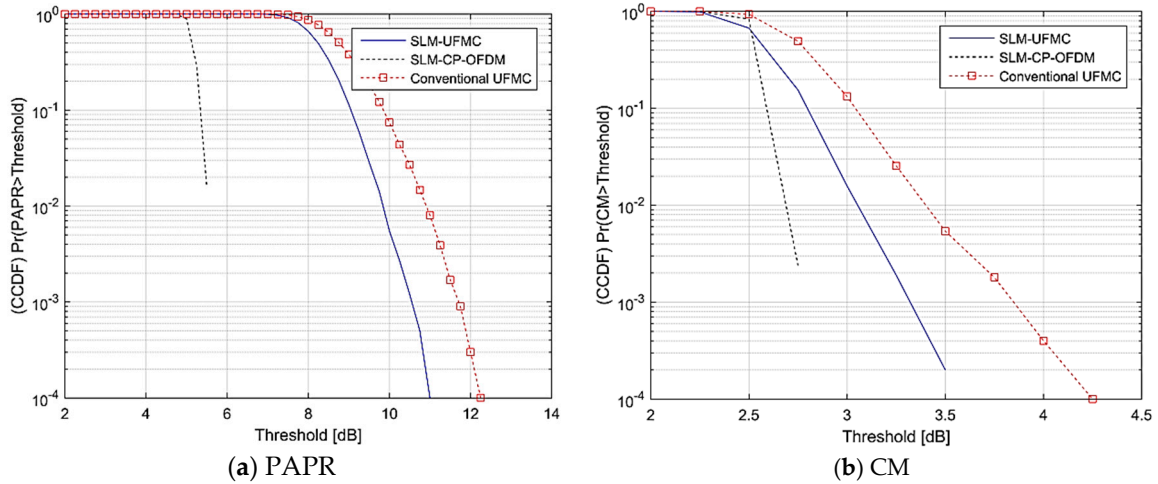


Figure 9. The 16-QAM and 6-PRV results of scenario 2.

Table 3. Simulation results of the second scenario (16-QAM), SLM-UFMC, and conventional UFMC.

No. of PRV	PAPR Before Reduction in dB	CM Before Reduction in dB	PAPR After Reduction in dB	CM After Reduction in dB	PAPR Reduction in dB	CM Reduction in dB
4	12	4	10.75	3.5	1.25	0.5
6	12.25	4.25	11	3.5	1.25	0.75
8	12.29	4.2	10.82	3.4	1.47	0.8

Figure 10a,b are the simulation results for the last case in the second scenario, which conducts 16-QAM with 8-PRV for the PAPR and CM, respectively. In Figure 10a, the PAPR is reduced from 12.29 dB, by 1.47 dB, while the CM is reduced by 0.8 dB. Eventually, increasing the number of PRV decreases the PAPR, but at the cost of increasing the complexity.

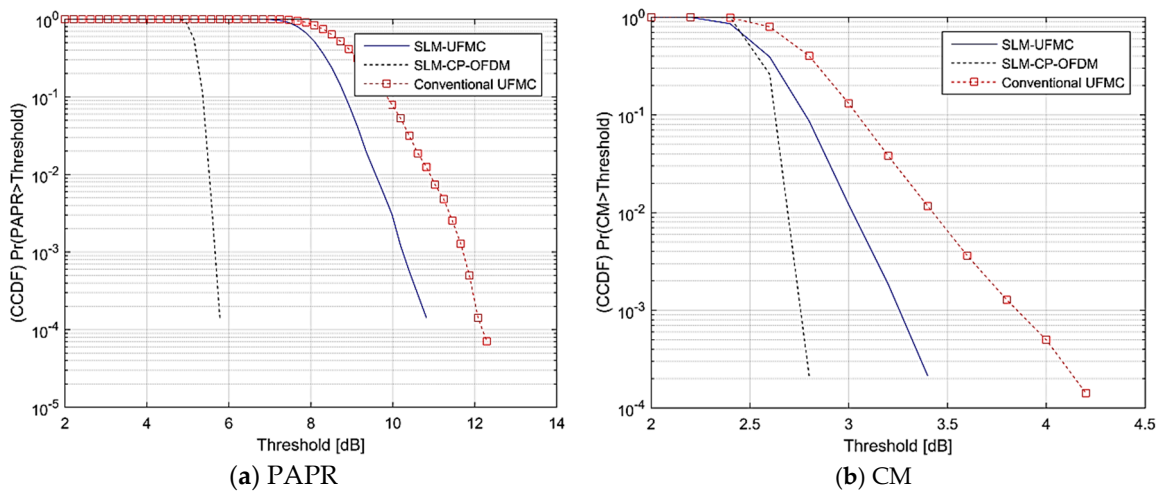


Figure 10. The 16-QAM and 8-PRV results of scenario 2.

The third scenario further increases the baseband mapping to 64-QAM. The first case of this scenario is the 4-PRV, which results in a PAPR of 12.25 dB and CM of 4.6 dB for the conventional UFMC.

The SLM-UFMC achieves less PAPR than 11 dB and CM of 3.4 dB from the conventional UFMC and SLM-UFMC, as shown in Figure 11a,b. Yet again, the SLM-CP-OFDM shows better results than the rest.

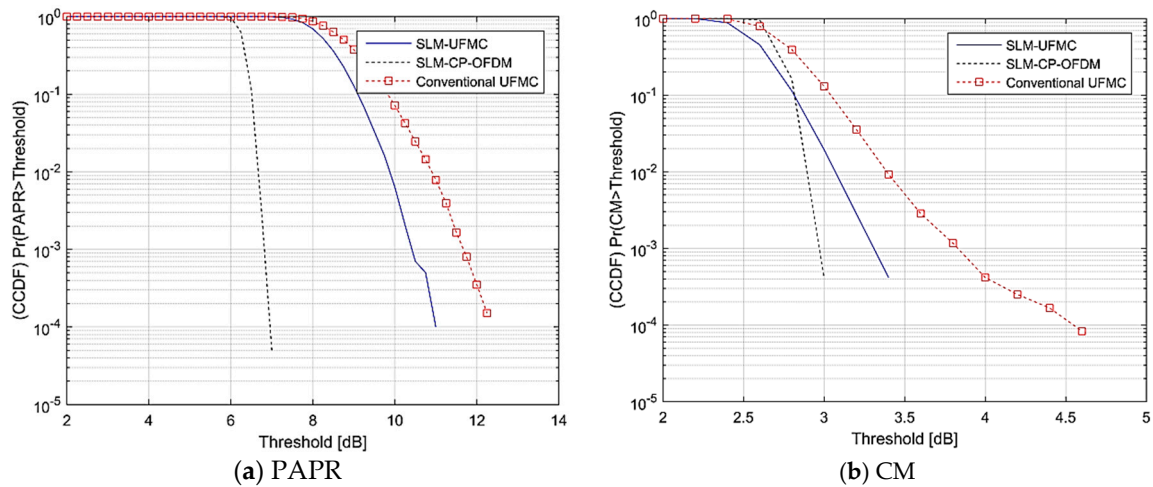


Figure 11. The 64-QAM and 4-PRV results of scenario 3.

The simulation with 6-PRV generally enhances the PAPR, in which it is reduced from 12.4 to 11.1 dB, as shown in Figure 11a. The CM has no improvement as compared with the 4-PRV, in which the same result of 1.2 dB is obtained, as shown in Figure 12b. Increasing the number of PRV to eight did not improve the PAPR and MC, as shown in Figure 13a,b. Thus, it is meaningless to increase the computational complexity by increasing the PRV. As shown in Table 4, the same behaviour of SLM-CP-OFDM is significantly shown, in which the CM is reduced by more than SLM-UFMC.

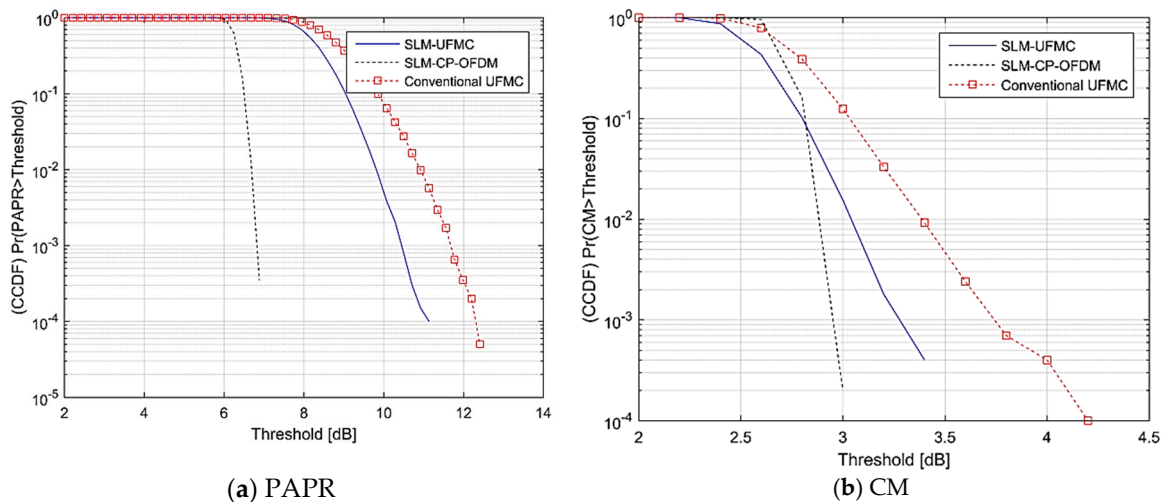


Figure 12. The 64-QAM and 6-PRV results of scenario 3.

In the last scenario, where the modulation order increased to 256-QAM, in which there are 8-binary bits incorporated in each subcarrier, the PAPR is reduced by 1.2 dB, 1.75 dB, and 1.9 dB for 4-PRV, 6-PRV, and 8-PRV, as shown in Figures 14–16 respectively. The CM is improved by 0.5, 0.6, and 0.8 dB. In particular, in the case of 4-PRV, the PAPR is reduced from 12.4 to 11.2 dB, and it is reduced from 12.5 to 10.75 dB in the case of 6-PRV. Finally, in the 8-PRV case, the PAPR of the UFMC is reduced from 12.3 to 10.4 dB after employing the SLM scheme. On the other hand, the CM is reduced from 4 to 3.5 dB in the 4-PRV case. For 6-PRV, the CM of the UFMC is reduced from 4 to 3.4 dB. In all of the cases of the last scenario, the SLM-CP-OFDM outperforms the other signals, but as stated previously,

at the expense of the spectrum efficiency degradation and the usage of different numerology cannot be employed using CP-OFDM. The results of the last scenario are presented in Table 5.

As a conclusion, Table 6 collectively lists the obtained results of the four-scenarios. It views the PAPR and CM reduction for each mapping order of 4-QAM, 16-QAM, 64-QAM, and 256-QAM. It can be observed that the PAPR decreased as the PRV number increased. On the other hand, the CM has the same attitude of the PAPR, but only the 64-QAM mapping does not change.

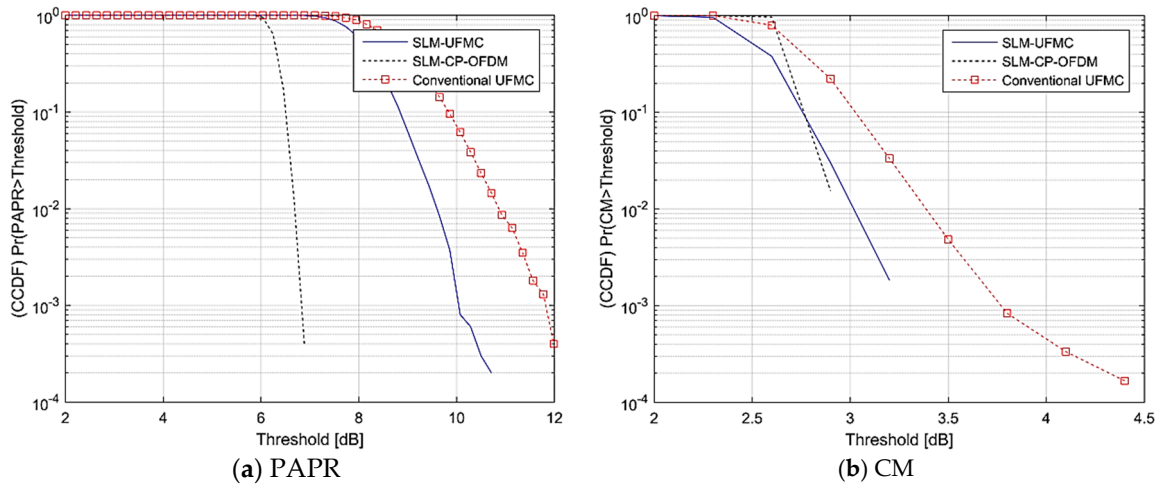


Figure 13. The 64-QAM and 8-PRV results of scenario 3.

Table 4. Simulation Results for the third scenario (64-QAM), SLM-UFMC, and conventional UFMC.

No. of PRV	PAPR Before Reduction in dB	CM Before Reduction in dB	PAPR After Reduction in dB	CM After Reduction in dB	PAPR Reduction in dB	CM Reduction in dB
4	12.25	4.6	11	3.4	1.25	1.2
6	12.4	4.2	11.1	3.4	1.3	1.2
8	12	4.4	10.7	3.2	1.3	1.2

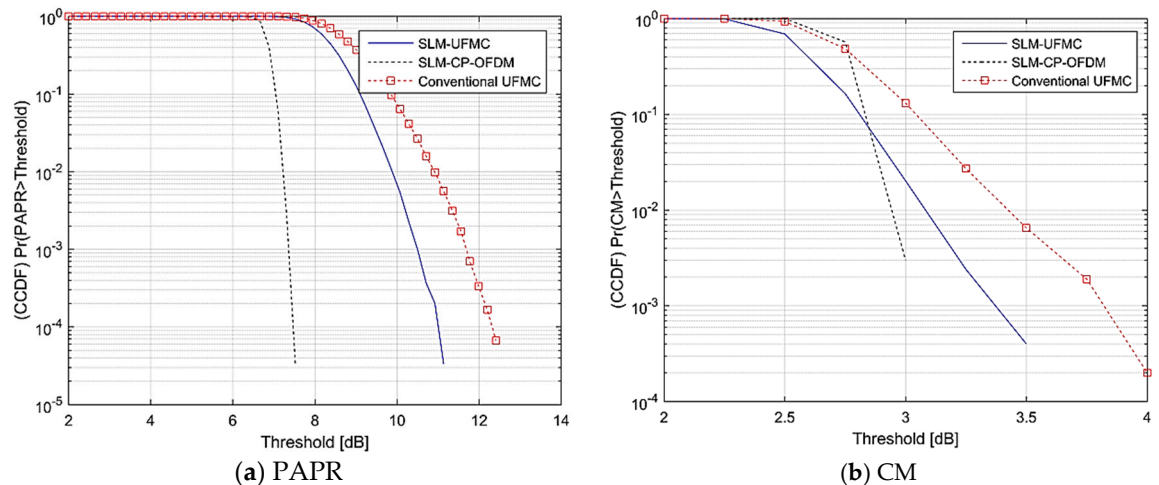


Figure 14. The 256-QAM and 4-PRV results of scenario 4.

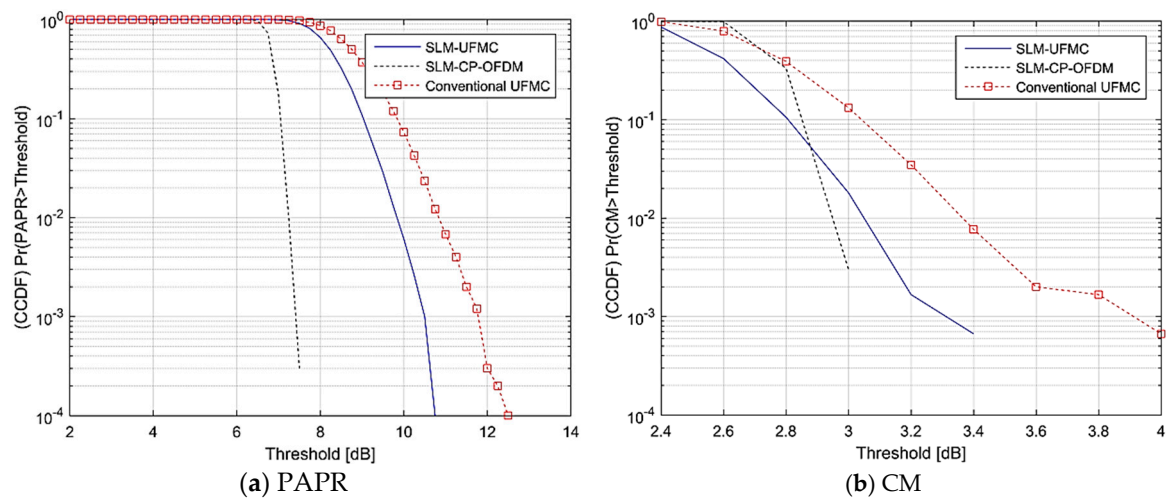


Figure 15. The 256-QAM and 6-PRV results of scenario 4.

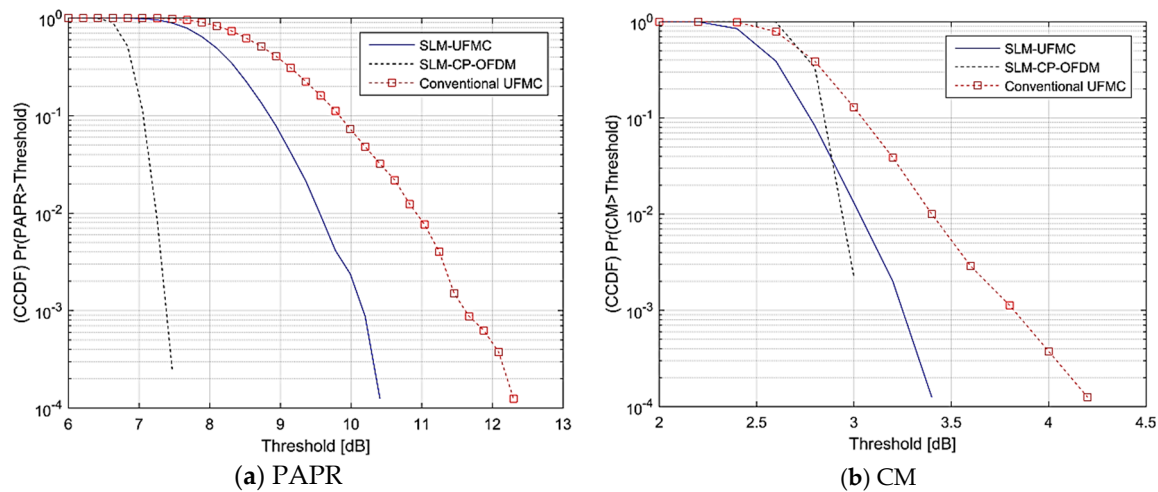


Figure 16. The 256-QAM and 8-PRV results of scenario 4.

Table 5. Simulation Results for the fourth scenario (256-QAM), SLM-UFMC, and conventional UFMC.

No. of PRV	PAPR Before Reduction in dB	CM Before Reduction in dB	PAPR After Reduction in dB	CM After Reduction in dB	PAPR Reduction in dB	CM Reduction in dB
4	12.4	4	11.2	3.5	1.2	0.5
6	12.5	4	10.75	3.4	1.75	0.6
8	12.3	4.2	10.4	3.4	1.9	0.8

Table 6. PAPR and CM reduction comparisons of the UFMC and SLM-UFMC for 4, 6, and 8-phase rotation.

Mapping Order	4-Phase Rotation Vectors		6-Phase Rotation Vectors		8-Phase Rotation Vectors	
	PAPR Reduction in dB	CM Reduction in dB	PAPR Reduction in dB	CM Reduction in dB	PAPR Reduction in dB	CM Reduction in dB
4-QAM	1	0.5	1	0.75	1.25	0.75
16-QAM	1.25	0.5	1.25	0.75	1.47	0.8
64-QAM	1.25	1.2	1.3	1.2	1.5	1.2
256-QAM	1.2	0.5	1.75	0.6	1.9	0.8

On the other hand, the number of multiplications and the number of additions depend on the size of the IFFT and the number of candidates utilized to reduce the PAPR/CM values. However, there is a trade-off between the two parameters. In the aforementioned scenarios, the numbers of multiplications operations are 9216, 13824, and 18432, for the CP-OFDM or conventional UFGC, 4-candidates SLM-UFGC, 6-candidates SLM-UFGC, and 8-candidates SLM-UFGC, respectively, as depicted in Table 7. The number of additions is simply divided into the above numbers by factor 2, as stated in Equations (22) and (23). Furthermore, the side information overhead increases with the increase in the number of candidates. According to Equation (24), the bits of side information are two, and three for the 4-candidates and 6-candidates or 8-candidates, respectively. Some applications in the 5G systems cannot be more complex than its standard form, while others may not care about the increased complexity, while the side information may be embedded in the transmitted data or send side information with faded subcarriers, which is out of the scope of this work. The results of Section 4 shows that as the number of PRV increases, the computational complexity increases. Accordingly, in Table 7, it can be observed that there is a trade-off between the computational complexity and the PAPR/CM, in which reducing the PAPR or CM increases the computational complexity.

**Table 7.** Calculation results of the computational complexity of the SLM-UFGC alongside the reduction in the PAPR and cm parameters in DB.

N	B	$\delta$	$\mu$ SLM	$\alpha$ SLM	PAPR Reduction (QAM)				CM Reduction (QAM)			
					4	16	64	256	4	16	64	256
512	4	2	9216	18432	1	1.25	1.25	1.2	0.5	0.5	1.2	0.5
512	6	3	13824	27648	1	1.25	1.3	1.75	0.75	0.75	1.2	0.6
512	8	3	18432	36864	1.25	1.47	1.5	1.9	0.75	0.8	1.2	0.8

The related work focused on four parameters of 5G networks which are computational complexity, PAPR, BER and side information. However, improving several parameters might negatively affect other parameters, for instance, improving the PAPR increase, the computational complexity and vice versa, as in [31] and [33]. Table 8 shows a comparison between our work with the benchmark of the related work based on this argument.

**Table 8.** Comparing our work with the benchmark.

Reference	Method/Waveform	Remarks
Jeon et al. [27]	<ul style="list-style-type: none"> <li>• SLM</li> <li>• OFDM</li> </ul>	<ul style="list-style-type: none"> <li>• Reduce the computational complexity without sacrificing the PAPR;</li> <li>• Slightly improve the bit error rate (BER);</li> <li>• Neglect the side information.</li> </ul>
Wang and Sheng-Ju Ku [30]	<ul style="list-style-type: none"> <li>• SLM</li> <li>• OFDM</li> </ul>	<ul style="list-style-type: none"> <li>• Reduce the computational complexity;</li> <li>• Limiting the transformed data rate (BER);</li> <li>• Neglect the side information.</li> </ul>
Hu et al. [31]	<ul style="list-style-type: none"> <li>• CPRV</li> <li>• SLM</li> <li>• OFDM</li> </ul>	<ul style="list-style-type: none"> <li>• Reduce the PAPR;</li> <li>• Increase the computational complexity;</li> <li>• Neglect the side information.</li> </ul>
Wang and Akansu [33]	<ul style="list-style-type: none"> <li>• OFDM</li> <li>• SLM</li> </ul>	<ul style="list-style-type: none"> <li>• Reduce the computational complexity;</li> <li>• Increase the PAPR;</li> <li>• Neglect the side information.</li> </ul>
Hu et al. [35]	<ul style="list-style-type: none"> <li>• SFBC</li> <li>• Multiple-input-multiple-output (MIMO)-OFDM</li> </ul>	<ul style="list-style-type: none"> <li>• Reduce the computational complexity;</li> <li>• Reduce the PAPR;</li> <li>• Neglect the side information;</li> <li>• Increase the BER.</li> </ul>



Table 8. Cont.

Reference	Method/Waveform	Remarks
Skrzypczak, et al. [20]	<ul style="list-style-type: none"> <li>• SLM</li> <li>• OFDM</li> </ul>	<ul style="list-style-type: none"> <li>• Reduce the PAPR;</li> <li>• Neglect the BER;</li> <li>• Neglect the computational complexity.</li> </ul>
Yang Zhou et al. [38]	<ul style="list-style-type: none"> <li>• OFDM</li> <li>• alternative-signal</li> </ul>	<ul style="list-style-type: none"> <li>• Reduce the PAPR;</li> <li>• Reduce the computational complexity;</li> <li>• Neglect the BER.</li> </ul>
Our Approach	<ul style="list-style-type: none"> <li>• UPMC</li> <li>• SLM</li> </ul>	<ul style="list-style-type: none"> <li>• Reduce PAPR and CM;</li> <li>• Slightly Reduce the BER;</li> <li>• Neglect the side information;</li> <li>• Neglect the computational complexity.</li> </ul>

From the above table, we can observe that the popular waveform is OFDM, and the SLM has been applied to the OFDM to reduce the PAPR of this waveform. Subsequently, the UPMC is considered as a promising waveform for 5G technology because it has a lower latency and better BER than the OFDM, but it is more complex. Moreover, both OFDM and UPMC suffer from high PAPR. Additionally, the table shows that the SLM for the UPMC waveform has not been proposed and evaluated. Our approach combines SLM with UPMC (SLM-UPMC) and is able to reduce the PAPR, BER and CM, but it neglects the side information and computational complexity. Hence, this study indicates that SLM has better spectral efficiency and can be used to reduce the Inter-Carrier Interference (ICI) which is symmetrical with the improvement in the UPMC signals. Ultimately, the SLM-UPMC shows better performance and consumes lower power than the SLM-CP-OFDM and conventional UPMC. The limitation of this work is that it neglects the side information and computational complexity.

## 5. Conclusions

The selected mapping (SLM) method has been suggested in the previous work to reduce the PAPR/CM in the UPMC waveform, in which the signal is copied to B candidates. The candidate with lower PAPR/CM can be adopted or selected for data transmission. The SLM introduces additional computational complexity due to the multiple signal representation, to provide B candidates. Furthermore, side information needs to be sent, which reduces the average rate of successful message delivery. The benefit of using selected mapping is that the PAPR/CM capacity is noticeably reduced without degrading the BER performance of the system. Thus, the reduction gain can be increased with the increment of the number of PRV, but this comes with the expense of high computational complexity. The testing results show that the PAPR can be reduced by 1.25 dB and the CM by 0.75 dB when the mapping order is 4-QAM in the 8-PRV case. The 16-QAM achieves the reduction of 1.47 dB PAPR and 0.8 dB CM. Finally, the 64-QAM achieves the reduction of 1.5 dB PAPR and 1.2 dB CM and the 256-QAM achieves the reduction of 1.9 dB PAPR and 0.8 dB CM. The contribution of this work is reducing the PAPR and CM for UPMC waveform by using the SLM technique, without degradation the BER. It is found from the results that there is symmetry between the UPMC improvement needs and the SLM solution. The limitation of this solution is increasing the computational complexity and neglecting side information. The future work considers reducing the computational complexity by using a Dummy Sequence Insertion (DSI) technique and utilizing side information within data transition.

**Author Contributions:** We would like to declare that all authors contributed equally to this manuscript. All authors have read and agreed to the published version of the manuscript.

**Funding:** This research was funded by Universiti Tenaga Nasional under Internal Research Grant OPEX type RJO10517919 iRMC Publication Fund and the Deanship of Scientific Research at Umm Al-Qura University for supporting this work by grant code: 19-COM-1-01-0015.

**Acknowledgments:** This research was partially funded by Universiti Tenaga Nasional under Internal Research Grant OPEX type RJO10517919 iRMC Publication Fund. The authors would also like to thank the Deanship of Scientific Research at Umm Al-Qura University for supporting this work by grant code: 19-COM-1-01-0015.

**Conflicts of Interest:** The authors declare no conflict of interest.

## References

1. Andrews, J.G.; Buzzi, S.; Choi, W.; Hanly, S.; Lozano, A.; Soong, A.C.K.; Zhang, J.C. What Will 5G Be? *arXiv* **2014**, arXiv:1405.2957. [[CrossRef](#)]
2. Al-Jawhar, Y.A.; Ramli, K.N.; Mustapha, A.; Mostafa, S.A.; Shah, N.S.M.; Taher, M.A. Reducing PAPR with Low Complexity for 4G and 5G Waveform Designs. *IEEE Access* **2019**, *7*, 97673–97688. [[CrossRef](#)]
3. Sexton, C.; Kaminski, N.J.; Marquez-Barja, J.M.; Marchetti, N.; Da Silva, L.A. 5G: Adaptable Networks Enabled by Versatile Radio Access Technologies. *IEEE Commun. Surv. Tutor.* **2017**, *19*, 688–720. [[CrossRef](#)]
4. Agiwal, M.; Roy, A.; Saxena, N. Next Generation 5G Wireless Networks: A Comprehensive Survey. *IEEE Commun. Surv. Tutor.* **2016**, *18*, 1617–1655. [[CrossRef](#)]
5. Medjahdi, Y.; Traverso, S.; Gerzaguet, R.; Shaiek, H.; Zayani, R.; Demmer, D.; Zakaria, R.; Dore, J.B.; Mabrouk, M.B.; Le Ruyet, D.; et al. On the Road to 5G: Comparative Study of Physical Layer in MTC Context. *IEEE Access.* **2017**, *5*, 26556–26581. [[CrossRef](#)]
6. Tao, Y.; Liu, L.; Liu, S.; Zhang, Z. A Survey: Several Technologies of Non-Orthogonal Transmission for 5G. *China Commun.* **2015**, *12*, 1–15. [[CrossRef](#)]
7. Nissel, R.; Schwarz, S.; Rup, M. Filter Bank Multicarrier Modulation Schemes for Future Mobile Communications. *IEEE J. Sel. Areas Commun.* **2017**, *35*, 1768–1782. [[CrossRef](#)]
8. Sheikh, J.A.; Mir, Z.I.; Parah, S.A.; Bhat, G.M. A New Filter Bank Multicarrier (FBMC) Based Cognitive Radio for 5G Networks Using Optimization Techniques. *Wirel. Pers. Commun.* **2020**. [[CrossRef](#)]
9. Farhang-Boroujeny, B. OFDM Versus Filter Bank Multicarrier. *IEEE Signal. Process. Mag.* **2011**, *28*, 92–112. [[CrossRef](#)]
10. Abdoli, J.; Jia, M.; Jianglei Ma, J. Filtered OFDM: A New Waveform for Future Wireless Systems. In Proceedings of the IEEE 16th International Workshop on Signal Processing Advances in Wireless Communications (SPAWC), Stockholm, Sweden, 28 June–1 July 2015; IEEE: Piscataway, NJ, USA, 2015; pp. 66–70.
11. Wild, T.; Schaich, F.; Yejian Chen, Y. 5G Air Interface Design Based on Universal Filtered (UF-) OFDM. In Proceedings of the 19th International Conference on Digital Signal. Processing (DSP), Hong Kong, China, 20–23 August 2014; IEEE: Piscataway, NJ, USA, 2014; pp. 699–704.
12. Wunder, G.; Fischer, R.F.; Boche, H.; Litsyn, S.; No, J.S. The PAPR Problem in OFDM Transmission: New Directions for a Long-Lasting Problem. *IEEE Signal. Process. Mag.* **2013**, *30*, 130–144. [[CrossRef](#)]
13. Chafii, M.; Palicot, J.; Gribonval, R.; Bader, F. A Necessary Condition for Waveforms with Better PAPR Than OFDM. *IEEE Trans. Commun.* **2016**, *64*, 3395–3405. [[CrossRef](#)]
14. Markku, R.; Yli-Kaakinen, J.; Valkama, M. Power Amplifier Effects on Frequency Localized 5G Candidate Waveforms. In Proceedings of the 22nd European Wireless Conference, Oulu, Finland, 18–20 May 2016; IEEE: Piscataway, NJ, USA, 2016; pp. 1–5.
15. Sendrei, L.; Marchevský, S.; Michailow, N.; Fettweis, G. Iterative Receiver for Clipped GFDM Signals. In Proceedings of the 24th International Conference Radioelektronika, Bratislava, Slovakia, 15–16 April 2014; IEEE: Piscataway, NJ, USA, 2014; pp. 1–4.
16. Rahmatallah, Y.; Mohan, S. Peak-To-Average Power Ratio Reduction in OFDM Systems: A Survey and Taxonomy. *IEEE Commun. Surv. Tutor.* **2013**, *15*, 1567–1592. [[CrossRef](#)]
17. Jiang, T.; Yang, Y.; Song, Y.H. Exponential Companding Technique for PAPR Reduction in OFDM Systems. *IEEE Trans. Broadcasting* **2005**, *51*, 244–248. [[CrossRef](#)]
18. Omid, M.J.; Minasian, A.; Saeedi-Sourck, H.; Kasiri, K.; Hosseini, I. PAPR Reduction in OFDM Systems: Polynomial-Based Compressing and Iterative Expanding. *Wirel. Pers. Commun.* **2014**, *75*, 103–118. [[CrossRef](#)]
19. Gopal, R.; Kumar Patra, S. Combining Tone Injection and Companding Techniques for PAPR Reduction of FBMC-OQAM System. In Proceedings of the Global Conference on Communication Technologies (GCCT), Thuckalay, India, 23–24 April 2015; IEEE: Piscataway, NJ, USA, 2015; pp. 709–713.
20. Skrzypczak, A.; Javaudin, J.P.; Siohan, P. Reduction of the Peak-to-Average Power Ratio for the OFDM/OQAM Modulation. In Proceedings of the IEEE 63rd Vehicular Technology Conference, Melbourne, Australia, 7–10 May 2006; IEEE: Piscataway, NJ, USA, 2006; Volume 4, pp. 2018–2022.

21. Skrzypczak, A.; Javaudin, J.P.; Siohan, P. Overlapped Selective Mapping for Pulse-Shaped Multi-Carrier Modulations. In Proceedings of the IEEE Vehicular Technology Conference, Montreal, QC, Canada, 25–28 September 2006; IEEE: Piscataway, NJ, USA, 2006; pp. 1–5.
22. Shukla, J.; Joshi, A.; Tyagi, R. PAPR Analysis of OFDM System Using AI Based Multiple Signal Representation Methods. *Telecommun. Comput. Electron. Control* **2019**, *17*, 2983. [[CrossRef](#)]
23. Müller, S.H.; Huber, J.B. OFDM with Reduced Peak-to-Average Power Ratio by Optimum Combination of Partial Transmit Sequences. *Electron. Lett.* **1997**, *33*, 368. [[CrossRef](#)]
24. Bäuml, R.W.; Fischer, R.F.H.; Huber, J.B. Reducing the Peak-to-Average Power Ratio of Multicarrier Modulation by Selected Mapping. *Electron. Lett.* **1996**, *32*, 2056. [[CrossRef](#)]
25. Joo, H.S.; Heo, S.J.; Jeon, H.B.; No, J.S.; Shin, D.J. A New Blind SLM Scheme with Low Decoding Complexity for OFDM Systems. *IEEE Trans. Broadcast.* **2012**, *58*, 669–676. [[CrossRef](#)]
26. Ji, J.; Ren, G.; Zhang, H. A Semi-Blind SLM Scheme for PAPR Reduction in OFDM Systems with Low-Complexity Transceiver. *IEEE Trans. Veh. Technol.* **2015**, *64*, 2698–2703. [[CrossRef](#)]
27. Jeon, H.B.; No, J.S.; Shin, D.J. A Low-Complexity SLM Scheme Using Additive Mapping Sequences for PAPR Reduction of OFDM Signals. *IEEE Trans. Broadcast.* **2011**, *57*, 866–875. [[CrossRef](#)]
28. Tsai, Y.R.; Lin, C.H.; Chen, Y.C. A Low-Complexity SLM Approach Based on Time-Domain Sub-Block Conversion Matrices for OFDM PAPR Reduction. In Proceedings of the IEEE Symposium on Computers and Communications (ISCC), Kerkyra, Greece, 28 June–1 July 2011; IEEE: Piscataway, NJ, USA, 2011; pp. 579–584.
29. Yoo, H.; Guilloud, F.; Pyndiah, R. Low Complexity SLM Technique with an Interleaver-Butterfly Ensemble for PAPR Reduction of Power Limited OFDM System. In Proceedings of the IEEE 73rd Vehicular Technology Conference (VTC Spring), Yokohama, Japan, 15–18 May 2011; IEEE: Piscataway, NJ, USA, 2011; pp. 1–5.
30. Wang, C.L.; Ku, S.J. Novel Conversion Matrices for Simplifying the IFFT Computation of an SLM-Based PAPR Reduction Scheme for OFDM Systems. *IEEE Trans. Commun.* **2009**, *57*, 1903–1907. [[CrossRef](#)]
31. Hu, W.; Yang, X.; Hu, X. Chaos-Based Selected Mapping Scheme for Physical Layer Security in OFDM-PON. *Electron. Lett.* **2015**, *51*, 1429–1431. [[CrossRef](#)]
32. Lim, D.W.; Heo, S.J.; No, J.S.; Chung, H. On the Phase Sequence Set of SLM OFDM Scheme for a Crest Factor Reduction. *IEEE Trans. Signal Process.* **2006**, *54*, 1931–1935. [[CrossRef](#)]
33. Yuewen, W.; Akansu, A.N. Low-Complexity Peak-to-Average Power Ratio Reduction Method for Orthogonal Frequency-Division Multiplexing Communications. *IET Commun.* **2015**, *9*, 2153–2159. [[CrossRef](#)]
34. Wang, S.H.; Lee, K.C.; Li, C.P. A Low-Complexity Architecture for PAPR Reduction in OFDM Systems with Near-Optimal Performance. *IEEE Trans. Veh. Technol.* **2016**, *65*, 169–179. [[CrossRef](#)]
35. Hu, W.W.; Huang, W.J.; Ciou, Y.C.; Li, C.P. Reduction of PAPR Without Side Information for SFBC MIMO-OFDM Systems. *IEEE Trans. Broadcast.* **2019**, *65*, 316–325. [[CrossRef](#)]
36. Bulusu, S.K.C.; Shaiek, H.; Roviras, D.; Zayani, R. Reduction of PAPR for FBMC-OQAM Systems Using Dispersive SLM Technique. In Proceedings of the 11th International Symposium on Wireless Communications Systems (ISWCS), Barcelona, Spain, 26–29 August 2014; IEEE: Piscataway, NJ, USA, 2014; pp. 568–572. [[CrossRef](#)]
37. Krishna Chaitanya Bulusu, S.S.; Shaiek, H.; Roviras, D. Potency of Trellis-Based SLM over Symbol-by-Symbol Approach in Reducing PAPR for FBMC-OQAM Signals. In Proceedings of the IEEE International Conference on Communications (ICC), London, UK, 8–12 June 2015; IEEE: Piscataway, NJ, USA, 2015; pp. 4757–4762. [[CrossRef](#)]
38. Zhou, Y.; Jiang, T.; Huang, C.; Cui, S. Peak-to-Average Power Ratio Reduction for OFDM/OQAM Signals via Alternative-Signal Method. *IEEE Trans. Veh. Technol.* **2014**, *63*, 494–499. [[CrossRef](#)]
39. Kim, H.; Rautio, T. Weighted Selective Mapping Algorithm for FBMC-OQAM Systems. In Proceedings of the International Conference on Information and Communication Technology Convergence (ICTC), Jeju, Korea, 19–21 October 2016; IEEE: Piscataway, NJ, USA, 2016; pp. 214–219.
40. Afrasiabi-Gorgani, S.; Wunder, G. The Method of Conditional Expectations for PAPR and Cubic Metric Reduction. *arXiv* **2020**, arXiv:1909.10639.
41. Eli-Chukwu, N.C.; Onoh, G.N. Experimental Study on the Impact of Weather Conditions on Wide Code Division Multiple Access Signals in Nigeria. *Eng. Tech. Appl. Sci. Res.* **2019**, *9*, 4.
42. Behravan, A.; Eriksson, T. Some Statistical Properties of Multicarrier Signals and Related Measures. In Proceedings of the IEEE 63rd Vehicular Technology Conference, Melbourne, Australia, 7–10 May 2006; IEEE: Piscataway, NJ, USA, 2006; pp. 1854–1858.

43. Wu, M.; Qiu, Z. Power De-Rating Reduction for DFT-S-OFDM System. In Proceedings of the IET International Conference on Wireless Mobile and Multimedia Networks (ICWMMN), Hangzhou, China, 6–9 November 2006; Institute of Engineering and Technology: Stevenage, UK, 2006; p. 234.
44. Zhao, Y.; Liu, J.; Xie, S. Cubic Metric Reduction for Repetitive CAZAC Sequences in Frequency Domain. *arXiv* **2019**, arXiv:1910.11184.
45. Wang, X.; Mei, L.; Wang, Z.; Sha, X. Enhanced Clipping and Filtering with WFRFT for PAPR Reduction in OFDM Systems. In Proceedings of the IEEE Wireless Communications and Networking Conference (WCNC), Marrakesh, Morocco, 15–18 April 2019; IEEE: Piscataway, NJ, USA, 2019; pp. 1–6.
46. Setiawan, D.; Gunawan, D.; Sirat, D. Interference Analysis of Guard Band and Geographical Separation between DVB-T and E-UTRA in Digital Dividend UHF Band. In Proceedings of the International Conference on Instrumentation, Communication, Information Technology, and Biomedical Engineering (ICICI-BME), Bandung, Indonesia, 23–25 November 2009; IEEE: Piscataway, NJ, USA, 2009; pp. 1–6.
47. Hammoodi, A.; Audah, L.; Abas Taher, M. Green Coexistence for 5G Waveform Candidates: A Review. *IEEE Access*. **2019**, *7*, 10103–10126. [[CrossRef](#)]



© 2020 by the authors. Licensee MDPI, Basel, Switzerland. This article is an open access article distributed under the terms and conditions of the Creative Commons Attribution (CC BY) license (<http://creativecommons.org/licenses/by/4.0/>).